Organic Electronics 13 (2012) 1073–1080

Contents lists available at SciVerse ScienceDirect

Organic Electronics

journal homepage: www.elsevier.com/locate/orgel

Fourfold power efficiency improvement in organic light-emitting devices using an embedded nanocomposite scattering layer

Chih-Hao Chang [a,*], Kuo-Yan Chang [a], Yu-Jhong Lo [a], Shu-Jing Chang [a], Hsin-Hua Chang [b,*]

[a] Department of Photonics Engineering, Yuan Ze University, Chung-Li 32003, Taiwan, ROC
[b] Department of Electro-Optical Engineering, Vanung University, Chung-Li 32061, Taiwan, ROC

ARTICLE INFO

Article history:
Received 10 January 2012
Received in revised form 19 February 2012
Accepted 22 February 2012
Available online 12 March 2012

Keywords:
Internal extraction structures
Titanium oxide
Nanoparticles
Blue phosphorescent OLEDs

ABSTRACT

It has been demonstrated that internal extraction structures (IES) can be introduced in OLEDs to decrease the ratio of the waveguide mode and simultaneously increase the ratios of the substrate and radiation modes. In this study, titanium oxide (TiO_2) nanoparticles (NPs) combined with transparent photoresist (TPR) were utilized to form an embedded nanocomposite scattering layer between the indium-tin-oxide (ITO) and glass substrate, leading to a significant boost in the out-coupling efficiency of the OLEDs. Inside the nanocomposite scattering layer, NPs of different sizes served distinct functions. The 250 nm-TiO_2 particles were used to induce scattering and diminish the light reflection back to the ITO layer. On the other hand, the refractive index of the TPR can be increased by increasing the concentration of the 25 nm-TiO_2, which reduced the difference in the refractive index between the ITO and TPR and thus multiplied the amount of light entering into the scattering layer. By employing nanocomposite substrate with mixed dual-sized NPs, we obtained power efficiencies of the blue phosphorescent OLEDs that were about 4.3 times higher than that of the control device at the high luminance of 5×10^3 cd/m^2.

1. Introduction

Organic light-emitting devices (OLEDs) have attracted widespread attention due to their potential applications in displays and solid-state lighting (SSL) [1–2]. Due to the ever maturing fabrication techniques in small- and medium-sized display panels, a string of products have recently been launched in the markets for mobile phone and tablet PC to much acclaim. In sharp contrast to the rapid progress being made in the field of display, the prospects are much less optimistic in lighting, although a number of manufacturers have announced plans for mass production scheduled in a few years. The delays could be attributed to the immature technologies for phosphorescent materials and light-extraction. Adequate color rendering capability and sufficient lumen flux are essential for quality lighting. However, deep-blue or true-blue phosphors have proved insufficiently stable to overcome the lifetime issues until now [3]. These setbacks have thus forced researchers to adopt white OLEDs (WOLEDs) with inferior efficiencies by employing blue fluorescent materials [4]. Besides, WOLEDs need to be operated at a high current density to ensure an ample flux of light. Therefore, the ensuing limited efficiency and lifespan can be expected when OLEDs are driven with high-bias and non-stopped operations. The result is that WOLEDs have yet to make much headway in the current lighting markets.

In view of the present bottom-emitting OLED architecture, the generated light is classified into four types of modes in OLEDs: radiation mode, substrate mode, ITO/organic-waveguided modes, and surface plasmon mode [5]. The radiation mode generally makes up only about 25% of the light generated, and typically does not contribute significantly to the flux of the device. Once we are able to improve the radiation mode, the OLEDs will be able to

* Corresponding authors. Tel.: +886 3 4638800x7517; fax: +886 3 4514281.
E-mail addresses: chc@saturn.yzu.edu.tw (C.-H. Chang), hhua3@mail.vnu.edu.tw (H.-H. Chang).

1566-1199/$ - see front matter © 2012 Elsevier B.V. All rights reserved.
doi:10.1016/j.orgel.2012.02.017

operate under the condition of lower biases (or higher efficiencies), which will enhance the lifespan significantly. Several methods employing external extraction structures (EES) such as microlens array, luminaire, and shaped substrate have enjoyed great successes in recent years [6–8]. The out-coupling efficiencies of these techniques ranged from 1.5 to 1.8 times compare to the original performance in the forward direction. Further enhancement is limited because these external extraction structures targeted only the reduction of the substrate mode. More recently, researchers have instead focused on internal extraction structures (IES) to overcome this limitation [9–11]. Nevertheless, the additional structures inserted into the OLEDs structure will increase the difficulties in the sequential manufacturing. As such, there are much fewer scientific reports on embedded structures for light extraction compared with those for their EES counterparts.

For example, Matterson et al. showed that Bragg-scattering could be effectively applied to polymer light-emitting diodes through adopting a photoresist with periodic corrugation in 2001 [12]. In 2004, Do et al. demonstrated that over 50% light extraction efficiency from OLEDs could be realized by the insertion of a two-dimensional SiO_2/SiN*x* photonic crystal structure [13]. The improvement mainly resulted from the liberation of the photons trapped in the high-index guiding layers. In 2008, Sun and Forrest developed a new light extraction approach by embedding low-index grids [14]. Light rays with high angles and originally trapped by total internal reflection at the ITO/glass interface can now enter the low-index region, and are refracted in a direction towards the substrate's normal. By combining the microlens array, the group showed that a light extraction efficiency about 2.3 times that of original device could be achieved. In addition, Takezoe and co-workers successfully demonstrated in 2010 that spontaneously formed buckles can effectively increase the light extraction efficiency [15]. The power efficiency of the OLEDs was improved by a factor of 2.9 with triple buckling at high luminescence. More recently, Wu and co-workers developed a method utilizing internal scattering layers, and obtained enhancement in the optical out-coupling by up to about twofold [16]. The fabrication of nanocomposite scattering films is primarily based on solution-processing, which is relatively simple and convenient. However, the out-coupled light was limited because of the noticeable differences in the refractive index between the indium-tin-oxide (ITO) and the transparent photoresist (TPR). As such, there remains plenty of room for further improvement by reducing the total internal reflection at the ITO/photoresist interface.

Therefore, we report a method as demonstrated below in an attempt to increase the refractive index of the TPR by adopting small-sized nanoparticles (NPs). Furthermore, by combining titanium oxide (TiO_2) of two distinct sizes, one can fully utilize the nanocomposite scattering film in blue phosphorescent OLEDs (PhOLEDs) to obtain devices with a maximum external quantum efficiency of *ca.* 21% at 10^4 cd/m^2, which is undoubtedly comparable with state-of-the-art methods. This highly expedient and effective technique can potentially push WOLEDs close to commercialization.

2. Experimental details

2.1. Fabrication of the nanocomposite scattering films

For the purpose of light extraction, the primary requirements for the host material of the NPs are high transmittance and low absorption in the visible wavelength range. In addition, the surface flatness, hardness, adhesion and heat-resistant capability of the host materials can also significantly affect the sequential fabrication of the device. To meet the aforementioned stringent requirements, the transparent negative photoresist (EOC130), purchased from Everlight Chemical, was selected as the host material. TiO_2 nanoparticles were used as scattering objects because of their high refractive index ($n \sim 3.1$ at 475 nm) as well as varied sizes. The glass substrate (Eagle 2000), with a high transmittance of about 92% in the visible wavelength range, was purchased from Corning. The refractive index of the glass substrate is 1.517 at 435.8 nm.

The nanocomposite films were assembled in three steps. First, the mixed solution was prepared through mixing the appropriate concentrations of NPs and transparent photoresist (TPR). Second, to ensure that the NPs were able to overcome the strong van der Waals forces and were well dispersed in the TPR, the mixture was then ultrasonically shaken for 1 day and filtered. Third, the filtered mixture was spin-coated onto the glass substrate and then curried at 120 °C for 5 min. The thicknesses of the nanocomposite films were adjusted by controlling the spinning speed. In this study, two kinds of nanocomposite films were prepared, namely the single-sized TiO_2 NPs (Type-I substrates) and dual-sized TiO_2 NPs (Type-II substrates).

Both atomic force microscope (AFM, SEIKO SPA400-SPIWin) and scanning electron microscope (SEM, JEOL JSM-7600F) were employed to monitor the surface roughness and morphology before the ITO coating processes. Furthermore, we also characterized the diffusing properties of the nanocomposite substrate by a UV–Vis spectrophotometer equipped with/without an integrating sphere, including the total transmittance (T_{total}) and the direct transmittance (T_{direct}). The definition of T_{total} and T_{direct} were precisely outlined in the literature. Consequently, the diffuse transmittance $T_{diffuse}$ denotes the difference between the total transmittance and the direct transmittance and can be used to calculate the Haze ($T_{diffuse}/T_{total}$), a valuable indication of the optical scattering capability [16].

2.2. OLED fabrication and characterizations

Subsequently, the nanocomposite substrates were obtained through coating the transparent electrode ITO via radio frequency magnetron sputter deposition. Bottom-emitting OLEDs, which consist of multiple organic/metal layers sandwiched between the ITO anode and the top metal cathode, are typically fabricated as follows. The organic materials for the small molecules used were purchased from Nichem. All organic compounds utilized were subject to temperature-gradient sublimation under high vacuum before use. Additionally, the polymer material, poly(3,4-ethylenedioxythiophene):poly(styrenesulfonate) (pedot:pss, Clevios PVP CH 8000), was purchased from

Starck. The organic and metal layers were deposited by vacuum evaporation in a vacuum chamber with a base pressure of $<10^{-6}$ torr. The deposition system enabled the fabrication of the complete device structure without breaking vacuum. The deposition rate of the organic layers was kept at ~0.1 nm/s. The active area of the device was 2×2 mm^2, as defined by the shadow mask for cathode deposition. Current–voltage–luminance (*I–V–L*) characterization of the devices was performed using an Agilent 4156C semiconductor parameter analyzer and a Si photodiode calibrated with a Photo Research PR650. Electroluminescence spectra of the devices were recorded by using an ocean optics spectrometer. In view of the fact that blue emitters play a key role in the development of white OLEDs, we focused only on the blue OLEDs to simplify the issues involved. Consequently, the well-known blue iridium complex, iridium(III) bis[(4,6-di-fluorophenyl)-pyridinato-*N*,$C^{2'}$]picolinate (FIrpic), was used to fabricate the tested devices [17].

The same device structure of blue PhOLEDs was utilized here to ensure a fair comparison. According to our recent research findings, a high internal quantum efficiency can be achieved by combining FIrpic with the wide triplet gap host 1,3-bis(9-carbazolyl)benzene (mCP) [18]. The di-[4-(N,N-ditolyl-amino)-phenyl]cyclohexane (TAPC) and 1,3,5-tri[(3-pyridyl)-phen-3-yl]benzene (TmPyPB) were selected as the hole-transport layer and electron-transport layer respectively due to their high carrier transport and exciton confinement capabilities [19–20]. In addition, the conductive polymer, pedot:pss, holds a distinct advantage in facilitating the planarization of the ITO substrate, especially in substrates with nanocomposite films [21]. As a result, the device structure consisted of ITO (110 nm)/pedot:pss (~30 nm)/TAPC (10 nm)/mCP doped with 8 wt.% FIrpic (20 nm)/TmPyPB (50 nm)/LiF (0.8 nm)/Al (150 nm), where the LiF and aluminum were used as the electron-injection layer and cathode, respectively. The structural drawing of the materials and schematic structures of the tested blue PhOLEDs are shown in Fig. 1.

3. Results and discussions

3.1. Transmittance and refractive index of the nanocomposite films

When an additional TPR film was inserted between the ITO and glass substrate, the difference in the refractive index between the two would result in severe total internal reflections even though the surface of the TPR film was not particularly smooth. Fortunately, the refractive index of the TPR film is adjustable by mixing NPs with high refractive indices [22]. Because the larger NPs' sizes are similar to the wavelength of emissive light, the significant scattering phenomenon renders the refractive indices

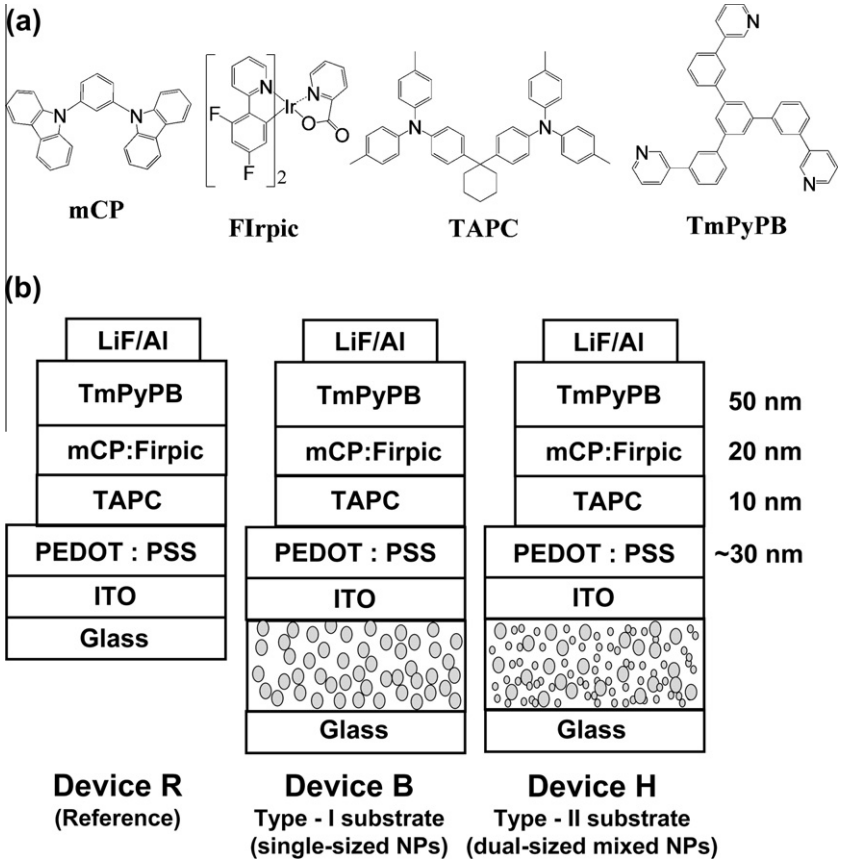

Fig. 1. The structural drawing of the materials and schematic structures of the tested blue phosphorescent OLEDs.

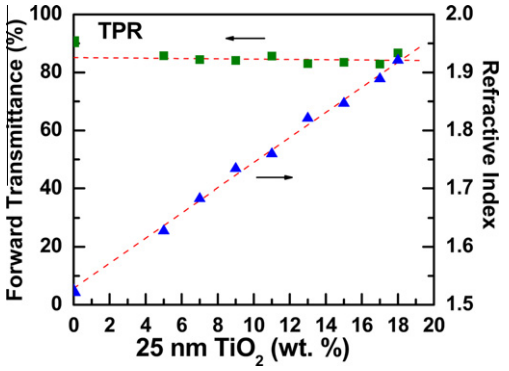

Fig. 2. The forward transmittances and the refractive indices of the nanocomposite films with different concentrations of 25 nm-NPs at the incident wavelength of 475 nm.

unmeasurable. In addition, considering the possible wavelength ranges of the OLED's emission, relatively smaller NPs of 25 nm in combination with TPR were adopted to avoid abrupt drops in the forward transmittance.

Thus, to gain further insights into the components of the device, we measured the forward (direct) transmittances and the refractive indices of the nanocomposite films with different concentrations of 25 nm-NPs at the incident wavelength of 475 nm (dominant wavelength of Flrpic), as shown in Fig. 2. The transmittances and refractive indices of pure TPR were recorded at 90.6% and 1.52, respectively. Moreover, the transmittances of the tested nanocomposite films were roughly independent of the NPs' concentrations and remained at a high level of about 85%. The rather high transmittance of nanocomposite film implied the poor scattering capability. On the other hand, by increasing the NPs' concentration in the nanocomposite films from 5 wt.% to 18 wt.%, the refractive index gradually increased from 1.63 to 1.92. Therefore, the use of 25 nm-NPs certainly helped to increase the refractive index of the TPR to match that of the ITO, thereby resulting in the mitigation of the total internal reflection between the ITO/TPR interfaces.

3.2. Surface morphology of the nanocomposite films

We named the three types of substrates used in the study were named as Type-R (Glass/ITO), Type-I (Glass/single-sized NPs mixed in TPR/ITO), and Type-II (Glass/dual-sized mixed NPs mixed in TPR /ITO). In a second set of substrates (i.e. Type-I), TiO_2 of different diameters (including 100, 250 and 400 nm) were also tested. The concentration of the mixed solution was fixed at a ratio of 0.6 g NPs to 4 g TPR. In addition, the spinning speed was fixed at 5000 rpm. based on past empirical parameters. The ingredients and related optical/morphological data of the nanocomposite films are summarized in Table 1. The Haze values of the Type-I substrates with 100 nm, 250 nm, and 400 nm-sized NPs were 6.90%, 96.16%, and 90.86%, respectively. On the other hand, the root mean square roughness (R_{rms}) of the corresponding Substrates A, B and C were 5.91 nm, 20.94 nm, and 19.60 nm, respectively. Thus, although the nanocomposite substrate containing 100 nm-NPs possessed smoothest surface, the lower Haze value indicated limited scattering capability. Furthermore, the Substrate B had similar roughness and higher Haze value compared to the Substrate C, which could be confirmed by means of the Mie theory [23]. As such, the 250 nm-NPs were selected and utilized in the Type-I and Type-II substrates. In addition, after the processes of ITO coating and OLED fabrication were completed, the experimental outcomes indicated that the nanocomposite films with 100 nm and 400 nm-NPs exhibited inferior scattering capabilities while devices with comparatively superior efficiencies were obtained by employing the 250 nm-NPs nanocomposite substrate. These results can be discerned from the SEM and AFM images. The characterizations with respect to the surface morphology were conducted before the ITO coating processes. The top-view and cross-section SEM images of the nanocomposite films with 250 nm-TiO_2 (Substrate B) are shown in Fig. 3(a). The images reveal clearly the NPs cluster and gulley formed after processing by thermal annealing. The NPs cluster contained roughly three to five particles of TiO_2, and the cluster size ranged from about 500 nm to 750 nm. Consequently, it stands to reason that the NPs with larger diameter (i.e. 400 nm-NPs) presumably induced severe aggregation of the NPs and concomitantly reduced the scattering capability [24]. Moreover, an undulating surface caused by the larger NPs was detrimental to the yield of the device fabrication. For improving the device performance, it is pertinent to choose particles with the size of 250 nm without compromising the roughness in the Type-I substrates.

Accordingly, based on the recipe of the Type-I mixtures described above, a new set of nanocomposite films, into which additional 25 nm-NPs were mixed, were fabricated to increase the refractive index of the TPR. The ingredients

Table 1
The ingredients and related optical/morphological properties of different nanocomposite substrates.

Substrate		Type-I			Type-II				
		A	B	C	D	E	F	G	H
TiO_2	100 nm (wt.%)	13	0	0	0	0	0	0	0
	250 nm (wt.%)	0	13	0	13	13	13	13	13
	400 nm (wt.%)	0	0	13	0	0	0	0	0
	25 nm (wt.%)	0	0	0	11	13	15	17	18
R_{rms} (nm)		5.91	20.94	19.60	13.25	5.79	12.14	13.61	16.10
Transmittance (@475 nm)	T_{direct} (%)	81.68	2.64	5.40	2.41	6.95	5.14	7.26	6.53
	T_{total} (%)	87.73	68.61	59.06	59.46	59.93	61.09	62.51	62.43
	$T_{diffuse}$ (%)	6.05	65.97	53.66	57.05	52.98	55.95	55.25	55.90
Haze (@475 nm) (%)		6.90	96.16	90.86	95.94	88.40	91.59	88.39	89.59

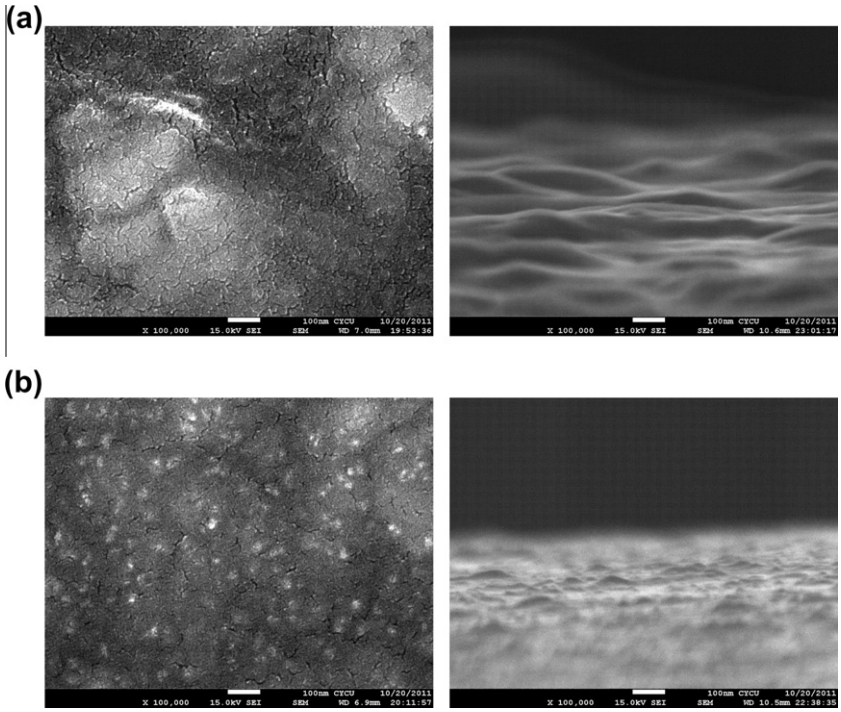

Fig. 3. (a) The top-view and cross-section SEM images of Substrate B with single-sized TiO_2; (b) the top-view and cross-section SEM images of Substrate E with dual-sized mixed TiO_2.

and related optical/morphological data of the Type-II nanocomposite films are also summarized in Table 1. The doping concentration of the 25 nm-NPs ranged from 11 wt.% to 18 wt.% (i.e. Substrate D–H) while the concentration of the 250 nm-NPs was fixed at 13 wt.%. From the Type-I and Type-II substrates, both Substrates B and H were selected to measure their thicknesses for a fair comparison. The thicknesses of the Substrates B and H were 1.07 μm and 1.66 μm, respectively. The viscosity of solution was proportional to the concentration of NPs [25]. Consequently, the thicker nanocomposite film resulted from higher concentration utilized in Substrate H. Fig. 3(b) shows the top-view and cross-section SEM images of Substrate E, which possessed the smoothest surface. Compared to the primitive nanocomposite films with single NPs (i.e. Substrate B); the NPs clusters were superseded by a uniform mixture of 25 nm-NPs. It is worth noting that these smaller NPs also played a role as effective dispersant in the nanocomposite films. Indeed, the scattered 25 nm-NPs filled up the pores and then stretched the distance between the 250 nm-NPs, thus drastically flatting the coarse surface, as was revealed in the cross-section SEM images [26]. In particular, the flattened surface of the Type-II nanocomposite films could be further confirmed by comparing the AFM images shown in Fig. 4(a) and (b). The root mean square surface roughness (R_{rms}) decreased as the concentration of 25 nm-NPs increased until 13 wt.%. However, once the concentration exceeded 13%, the surface once again became rough as a result of over-doping.

On the other hand, the nanocomposite films exhibited a boost in the forward transmittances at 475 nm when the doping concentrations of 25 nm-NPs exceeded 11 wt.% and stayed at as high as around 90%. This phenomenon was also reflected in the Haze of all tested samples. In other words, the scattering capabilities of the nanocomposite films were not strongly influenced by mixing additional 25 nm-NPs.

3.3. Electroluminescence characteristics of the devices

Due to previous reports demonstrating that the EL spectra of bottom-emitting OLEDs at different viewing angles were not altered by adding internal nanocomposite films, the electroluminescence (EL) efficiencies of the devices here reported were calculated on the basis of the Lambertian assumption [16]. The EL characteristics of blue PhOLEDs with different substrates are shown in Fig. 5, including Devices R (Type-R), B (Type-I), and H (Type-II). All devices exhibited bright emission of FIrpic, which indicates the presence of effective energy transfer between the host and guest. The small variations in the emission wavelength observed between devices were presumably associated with the concurrent changes in the optical effects. On the other hand, the current density–voltage (J–V) curves of the tested devices exhibited different behaviors although the architectures of the devices were the same and evaporation processes were performed together. As revealed from the J–V curves, the current density of the devices (namely Devices R, B, and H) at the operation voltage of 6 V were around 0.21, 0.56, and 3.02 mA/cm^2, respectively. The current density and luminance of devices with the Type-I substrate were higher than those of the device with the control

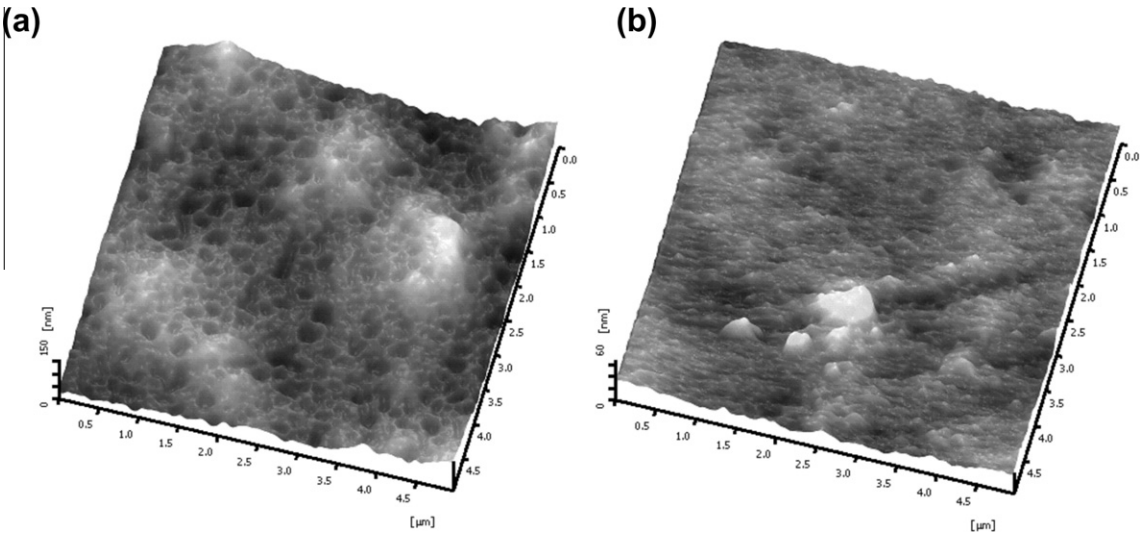

Fig. 4. (a) The AFM images of Substrate B with single-sized TiO_2; (b) the AFM images of Substrate E with dual-sized mixed TiO_2.

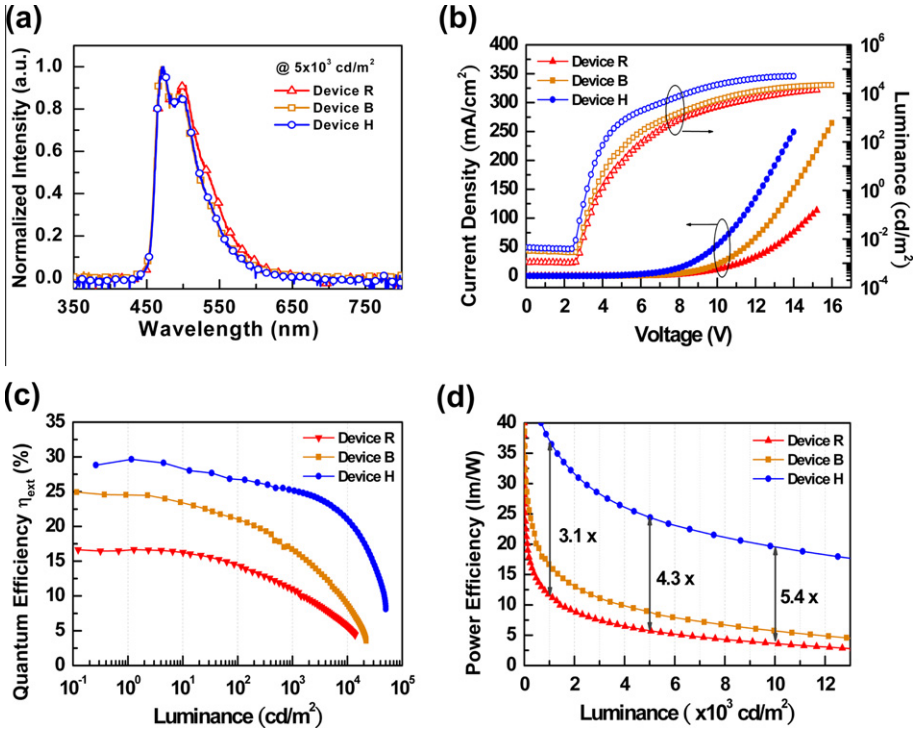

Fig. 5. (a) The normalized EL spectra; (b) current density–voltage-luminance (J–V–L) characteristics; (c) external quantum efficiency versus luminance; (d) power efficiency versus luminance of Devices R, B and H.

substrate, but lower than those of the devices with Type-II substrates. The larger current densities of tested devices with lumpy substrates mainly resulted from the enlarged active area due to the uneven surface, leading to higher current densities [15]. Therefore, though AFM images indicted that the Type-II substrates had smaller R_{rms}, the Type-II substrates were more corrugated than the Type-I substrates.

For the efficiencies in the applied forward bias, Device R exhibited a photon-to-electron efficiency at the practical luminance of 10^3 cd/m^2 of 11.0%, luminance efficiency (LE) of 30.5 cd/A, and power efficiency (PE) of 11.6 lm/W. Moreover, at the higher luminance of 5×10^3 cd/m^2 (or 10^4 cd/m^2) the efficiencies were reduced, with the EQE of 7.5% (5.6%), LE of 20.8 cd/A (15.6 cd/A), and PE of 5.7 lm/W

Table 2
The EL characteristics of tested devices with different substrates.

Device Substrate		Device R Ref. (Type-R)	Device B B (Type-I)	Device H H (Type-II)
External quantum efficiency (%) (enhancement)	[a]	11.0	16.7 (1.52×)	25.2 (2.29×)
	[b]	7.5	11.8 (1.58×)	23.0 (3.09×)
	[c]	5.6	8.8 (1.57×)	21.0 (3.75×)
Luminance efficiency (cd/A) (enhancement)	[a]	30.5	39.2 (1.29×)	62.9 (2.06×)
	[b]	20.8	27.6 (1.33×)	57.5 (2.77×)
	[c]	15.6	20.7 (1.32×)	52.5 (3.36×)
Power efficiency (lm/W) (enhancement)	[a]	11.6	16.6 (1.43×)	37.1 (3.20×)
	[b]	5.7	8.8 (1.53×)	24.5 (4.26×)
	[c]	3.6	5.7 (1.57×)	19.6 (5.40×)
V_{on} (V)	[d]	3.9	3.6	3.2
Max. luminance (cd/m^2)	[V]	13,889 (15.2 V)	22,084 (20.0 V)	50,421 (14.0 V)
CIE1931 coordinates	[a]	(0.181, 0.398)	(0.163, 0.373)	(0.157, 0.368)
	[b]	(0.181, 0.398)	(0.166, 0.356)	(0.158, 0.368)

[a] Measured at a luminance of 10^3 cd/m^2; [b] recorded at 5×10^3 cd/m^2; [c] recorded at 10^4 cd/m^2; [d] turn-on voltage measured at 1 cd/m^2.

(3.6 lm/W) (see Table 2). Nevertheless, the efficiency sustained at higher luminance was a crucial issue for the lighting purpose. Once the nanocomposite film was inserted into the OLEDs structure, the outcoupling efficiencies were enhanced due to the scattering phenomenon. At the higher luminance of 5×10^3 cd/m^2, the efficiencies of Device B were 11.8%, 27.6 cd/A, and 8.8 lm/W, around 1.5 times the corresponding values for Device R.

Evidently, further improvements in the efficiencies of the devices were obtained by utilizing Type-II substrates containing dual-sized NPs which provided scattering as well as refractive index matching functions. At the high luminance of 5×10^3 cd/m^2 (and 10^4 cd/m^2), in the forward direction, Device H exhibited efficiencies of up to 23.0% (21.0%), 57.5 cd/A (52.5 cd/A) and 24.5 lm/W (19.6 lm/W), confirming the superiority the Type-II substrates over the Type-R or Type-I substrates. An enhancement in the power efficiency of around 5.4 times at 10^4 cd/m^2 could be attained by employing substrate H with the appropriate recipe. In comparison to the efficiency roll-off behaviors of tested devices, the EQEs declined to one half at a current density ($J_{1/2}$) of 15.0, 14.3, and 81.0 mA/cm^2, for Devices R, B, and H, respectively. Similarly, the higher efficiencies observed in Device H were also attributed to the refractive index matching between the nanocomposite film and ITO film. The mitigated efficiency roll-off observed in Device H once again affirmed the significance of light extraction.

4. Conclusions

In summary, we have demonstrated that the out-coupling efficiency of OLEDs could be improved significantly by sophisticated substrate engineering. To better understand the functionality of the TiO_2 in the nanocomposite films, SEM and AFM images together with the transmittance/absorption spectra have been comprehensively studied. TiO_2 NPs of different particle sizes were shown to serve different functions. The 25 nm-NPs improved the refractive index of the TPR as well as flattened the surface of the nanocomposite film. On the other hand, the 250 nm-TiO_2 contributed to effective scattering. Through combining TiO_2 of different sizes in this study, we obtained a fabricated nanocomposite substrate with the multi-functionality of satisfactory transmittance, high refractive index, and great scattering capability. The efficiencies were remarkably enhanced to 25.2%, 62.9 cd/A, and 37.1 lm/W at 10^3 cd/m^2. In great contrast to the pristine ITO substrate, the power efficiency enhancement at the ultra-high luminance of 5×10^3 cd/m^2 was as high as 4.3 times for blue phosphorescent OLEDs utilizing an embedded nanocomposite film, thereby demonstrating the great potential of nanocomposite film for application in lighting.

Acknowledgements

The authors gratefully acknowledge the financial support from National Science Council of Taiwan (NSC 99-2221-E-155-035-MY3) and Ministry of Economic Affairs (100-EC-17-A-08-S1-042).

References

[1] C.-H. Chang, H.-C. Cheng, Y.-J. Lu, K.-C. Tien, H.-W. Lin, C.-L. Lin, C.-J. Yang, C.-C. Wu, Org. Electron. 11 (2010) 247–254.
[2] C.-H. Chang, K.-C. Tien, C.-C. Chen, M.-S. Lin, H.-C. Cheng, S.-H. Liu, C.-C. Wu, J.-Y. Hung, Y.-C. Chiu, Y. Chi, Org. Electron. 11 (2010) 412–418.
[3] C.-H. Chang, C.-C. Chen, C.-C. Wu, C.-H. Yang, Y. Chi, Org. Electron. 10 (2009) 1364–1371.
[4] Y. Sun, N.C. Giebink, H. Kanno, B. Ma, M.E. Thompson, S.R. Forrest, Nature 440 (2006) 908–912.
[5] C.-L. Lin, T.-Y. Cho, C.-H. Chang, C.-C. Wu, Appl. Phys. Lett. 88 (2006) 081114.
[6] S. Möller, S.R. Forrest, J. Appl. Phys. 91 (2002) 3324–3327.
[7] B.W. D'Andrade, J.J. Brown, Appl. Phys. Lett. 88 (2006) 192908.
[8] G. Gu, D.Z. Garbuzov, P.E. Burrows, S. Venkatesh, S.R. Forrest, M.E. Thompson, Opt. Lett. 22 (1997) 396–398.
[9] Y.-S. Tyan, Y.Q. Rao, X.F. Ren, R. Kesel, T.R. Cushman, W.J. Begley, N. Bhandari, SID Int. Symp. Dig. Tec. 40 (2009) 895–898.
[10] H.J. Peng, Y.L. Ho, X.J. Yu, H.S. Kwok, J. Appl. Phys. 96 (2004) 1649–1654.
[11] K. Hong, H.K. Yu, I. Lee, K. Kim, S. Kim, J.-J. Lee, Adv. Mater. 22 (2010) 4890–4894.
[12] B.J. Matterson, J.M. Lupton, A.F. Safonov, M.G. Salt, W.L. Barnes, I.D.W. Samuel, Adv. Mater. 13 (2001) 123–127.
[13] Y.R. Do, Y.-C. Kim, Y.-W. Song, Y.-H. Lee, J. Appl. Phys. 96 (2004) 7629–7636.
[14] Y. Sun, S.R. Forrest, Nat. Photonics 2 (2008) 483–487.
[15] W.H. Koo, S.M. Jeong, F. Araoka, K. Ishikawa, S. Nishimura, T. Toyooka, H. Takezoe, Nat. Photonics 4 (2010) 222–226.
[16] H.-W. Chang, K.-C. Tien, M.-H. Hsu, Y.-H. Huang, M.-S. Lin, C.-H. Tsai, Y.-T. Tsai, C.-C. Wu, J. Soc. Inf. Disp. 19 (2011) 196–204.

[17] C. Adachi, R.C. Kwong, P. Djurovich, V. Adamovich, M.A. Baldo, M.E. Thompson, S.R. Forrest, Appl. Phys. Lett. 79 (2001) 2082–2084.
[18] C.-H. Chang, Y.-S. Ding, P.-W. Hsieh, C.-P. Chang, W.-C. Lin, H.-H. Chang, Thin Solid Films 519 (2011) 7992–7997.
[19] P.M. Borsenberger, L. Pautmeier, R. Richert, H. Bassler, J. Chem. Phys. 94 (1991) 8276–8281.
[20] S.-J. Su, T. Chiba, T. Takeda, J. Kido, Adv. Mater. 20 (2008) 2125–2130.
[21] A. Elschner, F. Bruder, H.-W. Heuer, F. Jonas, A. Karbach, S. Kirchmeyer, S. Thurm, R. Wehrmann, Synth. Met. 111–112 (2000) 139–143.
[22] L.-H. Lee, W.-C. Chen, Chem. Mater. 13 (2001) 1137–1142.
[23] E.S. Thiele, R.H. French, J. Am. Ceram. Soc. 81 (1998) 469–479.
[24] C. Burda, X. Chen, R. Narayanan, M.A. El-Sayed, Chem. Rev. 105 (2005) 1025–1102.
[25] F.F. Lange, J. Am. Ceram. Soc. 72 (1989) 3–15.
[26] C.-C. Chang, W.-C. Chen, Chem. Mater. 14 (2002) 4242–4248.